

# Floquet Topological Frequency-Converting Amplifier

Adrian Parra-Rodríguez  <sup>1, 2, 3, 4, \*</sup> Miguel Clavero-Rubio  <sup>1</sup> Philippe Gigon  <sup>2, 3, 4</sup> Tomás Ramos  <sup>1</sup> Álvaro Gómez-León  <sup>1</sup> and Diego Porras  <sup>1, †</sup>

<sup>1</sup> Instituto de Física Fundamental (IFF), CSIC, Calle Serrano 113b, 28006 Madrid, Spain.

<sup>2</sup> Technical University of Munich, TUM School of Natural Sciences, Physics Department, 85748 Garching, Germany

<sup>3</sup> Walther-Meißner-Institut, Bayerische Akademie der Wissenschaften, 85748 Garching, Germany

<sup>4</sup> Munich Center for Quantum Science and Technology (MCQST), 80799 Munich, Germany

We introduce a driven-dissipative Floquet model in which a single harmonic oscillator with modulated frequency and decay realizes a non-Hermitian synthetic lattice with an effective electric field gradient in frequency space. Using the Floquet–Green’s function and its doubled-space representation, we identify a topological regime that supports directional amplification and frequency conversion, accurately captured by a local winding number. The underlying mode structure is well described by a Jackiw–Rebbi-like continuum theory with Dirac cones and solitonic zero modes in synthetic frequency. Our results establish a simple and experimentally feasible route to non-Hermitian topological amplification, naturally implementable in current quantum technologies such as superconducting circuits.

*Introduction.*— Topology has transformed our understanding of quantum systems by revealing new classes of states characterized not by local order parameters but by robust global topological invariants. Initially developed in the study of electronic systems, such as quantum Hall phases and topological insulators [1, 2], these ideas have spread across a broad range of physical settings. Topological photonics [3–5] extends these concepts to bosonic modes of light, enabling applications like robust control over signal propagation [6] and topological frequency combs [7]. In these systems, the combination of time-reversal symmetry breaking and non-Hermiticity due to intrinsic gain and loss leads to non-reciprocal transport and amplification [8–15]. A general theoretical framework based on topological band theory extended to non-Hermitian systems [16, 17] can be used to describe topological amplification in photonic lattices [18, 19]. In this approach, topological features emerge in the singular value spectrum of the coupling matrix in input-output theory, leading to directional amplification that remains robust in the presence of disorder [20–24].

Floquet systems, in which one or more parameters are periodically driven in time, further expand the landscape of topological phases. A prominent example is the class of Floquet topological insulators: nonequilibrium states of matter in which periodic driving induces novel topological phases that may be absent in equilibrium [25–28]. Such periodically driven systems are characterized by the emergence of one or more additional effective dimensions in frequency space. It has been shown that multiple incommensurate drives can simulate topological band structures in those synthetic dimensions, leading to topological frequency conversion [29] or quantized energy pumping between driving sources [30].

Latest advances have highlighted complementary mechanisms for engineering topology in driven photonic platforms. Time-Floquet modulation can induce non-reciprocal gain and directional amplification in zero-

dimensional parametric systems [31], static dissipation can be used to autonomously stabilize nonequilibrium Floquet states [32], and periodic modulation of a single microwave resonator has already been used to study synthetic Bloch-wave dynamics [33].

In this Letter, we demonstrate that periodically driven dissipation in addition to frequency modulation is sufficient to generate stable topological amplification and directional frequency conversion in an extremely minimal setting: a single bosonic mode subjected to a single periodic modulation of both its frequency and decay rate. The resulting driven-dissipative dynamics define a non-Hermitian lattice with an effective electric field gradient in frequency (Floquet–Sambe) space, locally analogous to a Floquet version of the Hatano–Nelson (HN) model [34] with asymmetric synthetic hopping between neighboring harmonics. A useful qualitative picture is provided by the Jackiw–Rebbi (JR) model [35], a one-dimensional Dirac equation with a sign-changing mass that hosts a topological zero mode at a domain wall, a minimal setting where index theorems apply [36, 37]. The topological properties of our effective Floquet lattice are revealed through the definition of a local topological invariant related to the system’s Green’s function, which determines amplification bandwidth, directionality, and robustness [38, 39].

Although our model echoes certain features of these earlier approaches, it operates through a fundamentally different physical mechanism. Here, topology is generated via competing coherent and dissipative Floquet couplings on a single-mode platform, thereby avoiding the need for multifrequency drives [29, 40, 41] or multimode architectures [31, 42]. Following well-established topological input–output theory [20], we extract the associated local topological invariant, compute a signal-to-noise ratio (SNR), and validate our predictions through exact numerical simulations. Finally, we propose an experimental implementation using superconducting circuits, where the required driven decay arises naturally via adi-

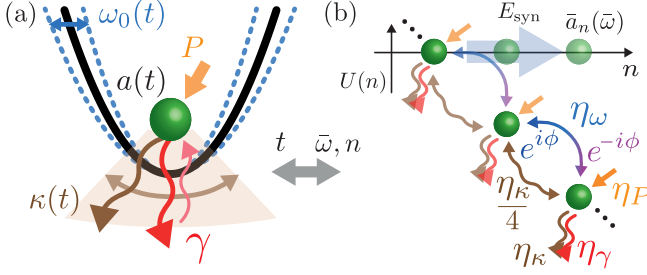


Figure 1. Sketch of the effective model: (a) A confined particle in a periodically driven harmonic potential  $\omega_0(t)$ , coupled to a static decay channel  $\gamma$  (also serving as a coherent drive port), a time-modulated decay channel  $\kappa(t)$ , and an incoherent pump  $P$ . (b) These periodic modulations implement a synthetic lattice with an effective constant electric field  $E_{\text{syn}}$  in frequency space, giving rise to directional amplification and frequency conversion due to time-reversal-symmetry breaking via asymmetric couplings.

abatic elimination of fast-dissipating ancillary modes.

*Model.*— We consider an open quantum system consisting of a single bosonic mode  $a$ , whose frequency  $\tilde{\omega}_0(t) = \omega_a + \omega_0(t)$  and decay rate  $\kappa(t)$  are periodically modulated, together with a static decay channel ( $\gamma = \eta_\gamma \Omega$ ) and an incoherent pump ( $P = \eta_P \Omega$ ); see Fig. 1(a). In the rotating frame with respect to the bare cavity frequency  $\omega_a$ , the dynamics are governed by the master equation

$$\mathcal{L}(\rho) = -i[\omega_0(t)a^\dagger a, \rho] + (\gamma + \kappa(t)) \mathcal{D}[a] + P \mathcal{D}[a^\dagger], \quad (1)$$

with the specific periodic modulations  $\omega_0(t) = 2\eta_\omega \Omega \cos(\Omega t + \phi)$  and  $\kappa(t) = 2\eta_\kappa \Omega \cos^2(\Omega t/2)$ . Here,  $\Omega$  denotes the common modulation frequency, and  $\eta_\alpha$  the modulation amplitudes. Without loss of generality, we assume throughout that  $\eta_\alpha > 0$  for all  $\alpha \in \{\omega, P, \kappa, \gamma\}$ .

The dissipative dynamics include a time-dependent decay rate, a constant incoherent pump, and a static loss channel, described by the superoperator  $\mathcal{D}[A] = A\rho A^\dagger - \frac{1}{2}A^\dagger A\rho - \frac{1}{2}\rho A^\dagger A$ . The modulated decay can be realized via a time-dependent coupling  $g_b(t)$  to a fast, strongly damped auxiliary mode  $b$  with decay rate  $\kappa_b \gg \gamma, g_b(t)$ , while the incoherent pump can be implemented through coupling to a fast-decaying auxiliary mode  $c$  ( $\kappa_c \gg \gamma, g_c$ ) via a parametric interaction (see Supplementary Material for details on the adiabatic elimination).

*Input–output theory.*— To analyze this dynamics, we employ quantum Langevin theory [20]. In the rotating frame, the single mode obeys

$$\dot{a}(t) = -i\omega_0(t)a(t) + \frac{P - (\gamma + \kappa(t))}{2}a(t) + \xi_{\text{in}}(t), \quad (2)$$

with the composite input operator  $\xi_{\text{in}}(t) = -\sqrt{\gamma}d_{\text{in}}(t) - \sqrt{\kappa(t)}w_{\text{in}}(t) + \sqrt{P}h_{\text{in}}^\dagger(t)$ , where  $d_{\text{in}}$ ,  $w_{\text{in}}$  and  $h_{\text{in}}$  are input noise operators for the  $\gamma$ ,  $\kappa(t)$ , and  $P$  independent channels, respectively.

Because the dynamics is linear and periodic, the system admits a Floquet pseudo-steady state. In this regime, the Fourier–Floquet expansion is well defined,

$$a(t) = \frac{1}{\sqrt{2\pi}} \int_0^\Omega d\bar{\omega} \sum_n \bar{a}_n(\bar{\omega}) e^{-i(\bar{\omega} + n\Omega)t}, \quad (3)$$

with  $\bar{\omega} \in [0, \Omega)$ , and analogously for the noise operators. In this basis, the equations of motion reduce to a linear algebra problem with formal solution  $\bar{a}_n(\bar{\omega}) = i \sum_m \mathbf{G}_{nm}(\bar{\omega}) \bar{\xi}_{\text{in},m}(\bar{\omega})$ , where the Floquet–Green’s function (FGF)  $\mathbf{G}(\bar{\omega}) \equiv (\bar{\omega} - \bar{\mathbf{H}})^{-1}$ . The effective dynamical matrix in harmonic space reads

$$\begin{aligned} \frac{\bar{\mathbf{H}}_{nm}}{\Omega} = & \left[ -n + i \left( \frac{\eta_P - \eta_\gamma - \eta_\kappa}{2} \right) \right] \delta_{n,m} \\ & + \left( \eta_\omega e^{i\phi} - \frac{i\eta_\kappa}{4} \right) \delta_{n,m-1} + \left( \eta_\omega e^{-i\phi} - \frac{i\eta_\kappa}{4} \right) \delta_{n,m+1}. \end{aligned} \quad (4)$$

This structure arises because both  $\omega_0(t)$  and  $\kappa(t)$  contain harmonics at frequency  $\Omega$ , leading to nearest-neighbor couplings in the synthetic lattice. This formulation, which locally resembles a Floquet generalization of the HN model, captures directional frequency conversion and amplification. The linear  $n$ -dependence of the diagonal term can be interpreted as a potential  $U(n) = -n$  induced by a synthetic electric field,  $|E_{\text{syn}}| = 1$  [27, 29].

The input noise vector is given by

$$\begin{aligned} \bar{\xi}_{\text{in},n}(\bar{\omega})/\sqrt{\Omega} = & \sqrt{\eta_P} \bar{h}_{\text{in},-n}^\dagger(-\bar{\omega}) - \sqrt{\eta_\gamma} \bar{d}_{\text{in},n}(\bar{\omega}) \\ & - \sqrt{\frac{\eta_\kappa}{2}} \left( \bar{w}_{\text{in},n}(\bar{\omega} + \frac{\Omega}{2}) + \bar{w}_{\text{in},n-1}(\bar{\omega} + \frac{\Omega}{2}) \right), \end{aligned} \quad (5)$$

for  $\bar{\omega} \leq \Omega/2$ . If  $\bar{\omega} > \Omega/2$ , the last term must be replaced by  $-\sqrt{\eta_\kappa/2}(\bar{w}_{\text{in},n+1}(\bar{\omega} - \Omega/2) + \bar{w}_{\text{in},n}(\bar{\omega} - \Omega/2))$ . Note that the last term introduces  $\Omega/2$  harmonics through the modulation of the coupling to the auxiliary cavity, but, assuming the latter is in vacuum, these harmonics do not contribute [43].

Using the input–output relation for the static port  $\gamma$ ,  $d_{\text{out}}(t) = d_{\text{in}}(t) + \sqrt{\gamma}a(t)$ , together with the linear solution above, we can express the output field in frequency space as  $\bar{d}_{\text{out},n}(\bar{\omega}) = \bar{d}_{\text{in},n}(\bar{\omega}) + i\sqrt{\gamma} \sum_m \mathbf{G}_{nm}(\bar{\omega}) \bar{\xi}_{\text{in},m}(\bar{\omega})$ . Substituting the input vector  $\bar{\xi}_{\text{in},m}(\bar{\omega})$ , we obtain

$$\begin{aligned} \bar{d}_{\text{out},n}(\bar{\omega}) = & \sum_m \mathbf{R}_{nm}(\bar{\omega}) \bar{d}_{\text{in},m}(\bar{\omega}) + \mathbf{P}_{nm}(\bar{\omega}) \bar{h}_{\text{in},-m}^\dagger(-\bar{\omega}) \\ & + \mathbf{Q}_{nm}(\bar{\omega}) \bar{w}_{\text{in},m}(\bar{\omega}), \end{aligned} \quad (6)$$

with effective scattering matrices  $\mathbf{R}_{nm}(\bar{\omega}) = \delta_{nm} - i\Omega\eta_\gamma \mathbf{G}_{nm}(\bar{\omega})$ , and  $\mathbf{P}_{nm}(\bar{\omega}) = i\Omega\sqrt{\eta_P\eta_\gamma} \mathbf{G}_{nm}(\bar{\omega})$ .  $\mathbf{Q}_{nm}(\bar{\omega})$  involves the  $\Omega/2$  sideband structure already mentioned and is omitted since that port is taken to be in vacuum.

These matrices contain all the necessary information to assess the device performance [44]. Given a coherent drive applied at port  $\gamma$ , the corresponding input field

is  $\langle d_{\text{in}}(t) \rangle = \alpha_d e^{-i\omega_d t}$  with  $\omega_d = \bar{\omega}_d + n_d \Omega$ , while all other inputs remain in vacuum. Using Eq. (6), the mean output field in the Floquet–Sambe basis is  $\langle \bar{d}_{\text{out},n}(\bar{\omega}) \rangle = \sqrt{2\pi} \alpha_d \mathbf{R}_{n,n_d}(\bar{\omega}) \delta(\bar{\omega} - \bar{\omega}_d)$ .

*Topological frequency conversion and amplification.*— The non-Hermitian Green’s function of linear systems such as ours is well known to be linked to an eigenvalue problem in a doubled space [18, 20, 22–24, 45]. Explicitly, the doubled Hermitian matrix

$$\mathcal{H}(\bar{\omega}) = \begin{pmatrix} 0 & \bar{\omega} - \tilde{\mathbf{H}} \\ \bar{\omega} - \tilde{\mathbf{H}}^\dagger & 0 \end{pmatrix}, \quad (7)$$

presents the eigensystem  $\mathcal{H}(\bar{\omega})(\mathbf{u}_l^T, \pm \mathbf{v}_l^T)^T = \pm E_l (\mathbf{u}_l^T, \pm \mathbf{v}_l^T)^T$ , so that the singular value decomposition (SVD) of the Green’s function reads  $\mathbf{G}(\bar{\omega}) = \sum_l \mathbf{v}_l \frac{1}{E_l} \mathbf{u}_l^\dagger$ , with  $E_l > 0$ . This correspondence establishes a link between input-output theory and TBT [20], thereby enabling the characterization of topological phases. In our case,  $\mathcal{H}(\bar{\omega})$  possesses chiral symmetry, and, in general, belongs to the AIII symmetry class of the Altland–Zirnbauer classification [46, 47], supporting directional frequency conversion and amplification via topologically protected edge states.

Since the full model is infinite in the harmonic index  $n \in \mathbb{Z}$ , we truncate to a finite synthetic frequency window  $|n| \leq N$ , justified by the spectral tilt  $-n\delta_{n,m}$  in Eq. (4) acting as a synthetic electric field that detunes distant sites. We denote the truncated matrix  $\tilde{\mathbf{H}}$  and impose periodic boundary conditions to define the discrete Fourier transform  $\tilde{a}_k = \frac{1}{\sqrt{2N+1}} \sum_{n=-N}^N e^{-ikn} \tilde{a}_n$ , where  $k = 2\pi m/(2N+1)$  with  $m \in [-N, N]$ . In this basis, the dynamical matrix becomes

$$\frac{\tilde{\mathbf{H}}_{kk'}}{\Omega} = \left( 2\eta_\omega \cos(k + \phi) - i \frac{\eta_\kappa}{2} \cos(k) \right) \delta_{kk'} + i \left( \frac{\eta_P - \eta_\gamma - \eta_\kappa}{2} \right) \delta_{kk'} - f_{kk'}, \quad (8)$$

with  $f_{kk'} = \frac{1}{2N+1} \sum_n n e^{-i(k-k')n}$  representing the tilt. Note that replacing  $f_{kk'}$  by a  $k$ -independent constant restores exact translation symmetry and reduces Eq. (8) to the non-Hermitian Hatano–Nelson model, whose phase diagram is well known. In the spirit of local topological markers [48], we use a local (frozen- $n$ ) approximation to retain the linear tilt while keeping a band picture, i.e., for each harmonic  $n$  we set  $f_{kk'} \rightarrow n \delta_{kk'}$  and analyze the resulting family of local Bloch Hamiltonians  $\tilde{\mathbf{H}}_k(n)$ . Within each slice  $(\bar{\omega}, n)$ , we then define a local winding number

$$\nu_n(\bar{\omega}) = \oint \frac{dk}{4\pi i} \text{Tr} \left[ \sigma_z \tilde{\mathbf{H}}_k^{-1} \partial_k \tilde{\mathbf{H}}_k \right], \quad (9)$$

following the standard definition of the Floquet winding invariant for chiral 1D systems [49]. In the doubled representation  $\tilde{\mathbf{H}}_k(n) = \mathbf{r}(k, n) \cdot \boldsymbol{\sigma}$ , with  $\boldsymbol{\sigma} = (\sigma_x, \sigma_y, \sigma_z)$ , and  $\mathbf{r}(k, n)$  encoding the Bloch vector.

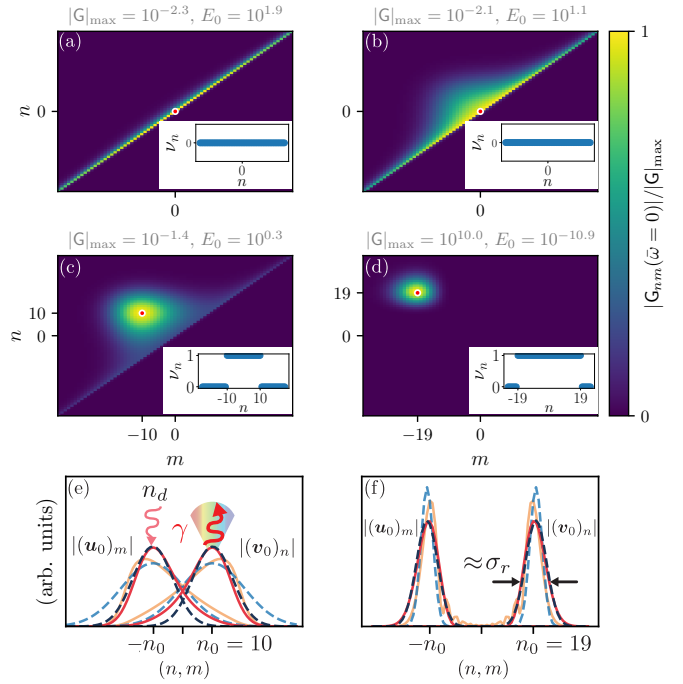


Figure 2. (a–d) The local winding number  $\nu_n(\bar{\omega})$  accurately predicts the topological region where  $|\mathbf{G}_{nm}(\bar{\omega})|$  reaches its off-diagonal maximum, signaling strong frequency conversion and, as  $\beta \rightarrow 1$ , enhanced amplification ( $E_0 \rightarrow 0$ ). Parameters are  $\eta_P = s \times (1, 9.5, 11.4, 19.5)$  with  $\eta_\omega = \eta_\kappa/s = \eta_\gamma/s = 10$ ,  $\phi = \pi/2$ ,  $\bar{\omega} = 0$ ,  $s = 3$ , and  $\Omega = 2\pi$ . (e,f) Normalized singular vectors for the parameter sets of panels (c) and (d), corresponding to  $\beta = 0.14$  and  $\beta = 0.95$  (topological regime). Curves for scaling parameters  $s = 1$  (orange, blue) and  $s = 3$  (red, black) are shown. Solid lines come from numerical diagonalization of Eq. (4), while dashed lines indicate the JR prediction (whose accuracy improves as  $s \rightarrow \infty$ ). (e) For an input signal at harmonic  $n_d$  from the  $\gamma$ -port, weighted by  $(\mathbf{u}_0)_{n_d}$ , the system’s steady state (and emitted spectrum  $\mathbf{d}_{\text{out},n}(\bar{\omega})$ ) contains harmonics given by  $(\mathbf{v}_0)_n$ , centered at  $n_0$  (with width  $\sigma_r \rightarrow \sqrt{\eta_\kappa/2}$  as  $\beta \rightarrow 1$ ), achieving maximum conversion when  $n_d = -n_0$ .

A nonzero local winding number  $\nu_n(\bar{\omega}) = \pm 1$  arises when the complex vector field  $\mathbf{r}(k, n)$ , encircles the origin in the synthetic Brillouin zone, occurring when  $(\bar{\omega}/\Omega + n)^2 \leq (2\eta_\omega)^2 \beta(2 - \beta)$ . Here, we have defined the normalized pump–loss imbalance parameter  $\beta \equiv (\eta_P - \eta_\gamma)/\eta_\kappa$ . This interval sets the topological frequency-conversion window, with its boundaries at  $n = \pm n_0 \equiv \pm 2\eta_\omega \sqrt{\beta(2 - \beta)}$ , nonempty for  $0 < \beta < 2$  (and  $\eta_\omega > 0$ ), with its maximum reached at  $\beta = 1$ , such that the window becomes  $\Delta n = 4\eta_\omega$ , corresponding to a frequency shift of  $4\eta_\omega \Omega$ .

In Fig. 2, we observe the main features of topological amplification and frequency conversion. In the topological phase, where  $\nu_n(\bar{\omega})$  is nontrivial, there is a quasi-zero singular value  $E_0$ , separated from the bulk singular values by a gap, leading to the approximation  $\mathbf{G}_{nm}(\bar{\omega}) \approx (\mathbf{v}_0)_n (\mathbf{u}_0^*)_m / E_0$ , where the FGF is dominated

by the zero channel. In panels (a–d), we plot the absolute value of the FGF for increasing values of  $\eta_P$ , such that, as we approach  $\beta \rightarrow 1$ , the system moves deeper into the topological phase, leading to smaller  $E_0$  values. This, in turn, enhances the FGF, giving rise to the phenomenon of topological amplification in the Floquet-Sambe space, and consequently, to frequency conversion. Chiefly, the region where  $\nu_n(\bar{\omega})$  is nontrivial pinpoints the indices at which  $G_{nm}$  attains its maximal weight, confirming the predictive power of the local approximation. Moreover, the sign of  $\nu_n$  directly indicates up- (+) or down- (–) frequency conversion.

Interestingly, further features of our amplifier, in particular, the input and output bandwidths can be quantitatively captured by the continuous JR theory. Within the topological region, the doubled matrix  $\tilde{\mathcal{H}}_k$  develops two Dirac cones located at  $(k, n) = \pm(k_0, -n_0)$ , with  $\cos k_0 = \beta - 1$  (and the previously defined  $n_0$ ). Linearizing around either cone, i.e.,  $k = \pm k_0 + \delta k$  and  $n = \mp n_0 + \delta n$ , yields an effective Dirac Hamiltonian whose spatially varying mass is  $m(\delta n) = \delta n$ . This supports Gaussian JR solitons centered at  $n = \pm n_0$ , with complex widths set by the slope (velocity) of the corresponding cone. In the ideal topological regime ( $\beta = 1$ ), these expressions simplify to  $n_0 \rightarrow 2\eta_\omega$  and a purely real Gaussian width  $\sigma_r = \sqrt{\eta_\kappa/2}$ , reproducing with excellent accuracy the numerically obtained zero-singular-value vectors. In Fig. 2(e, f), we show non-ideal cases with  $\beta \neq 1$  (corresponding to FGF in panels (c, d)). Further details on the JR approximation are given in the End Matter.

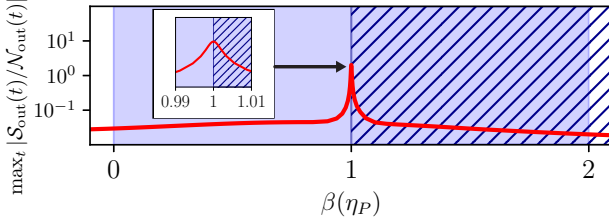


Figure 3. Maximum of the time-dependent SNR computed in the steady state as a function of  $\beta(\eta_P)$  [44]. The blue (dashed) region identifies the topological (unstable) regime. Parameters are  $\eta_\omega = \eta_\kappa = \eta_\gamma = 10$ ,  $\phi = \pi/2$ , and  $\eta_P \in (9, 30)$ .

*Stability and SNR.*— The topological criterion derived above determines when the doubled-space Hamiltonian supports zero-singular-value solitons, but this alone does not ensure dynamical stability. Stability is governed instead by the long-time behavior of the intracavity photon number, which obeys  $\frac{d}{dt}\langle a^\dagger a \rangle / \Omega = \eta_\kappa(\beta - 1)\langle a^\dagger a \rangle - \eta_\kappa \cos(\Omega t)\langle a^\dagger a \rangle + \eta_P$ , where the last term arises from the noise correlations of the pump channel. This quantity grows without bound whenever there is net energy gain, i.e., whenever  $\beta > 1$ . Near the ideal topological regime,

the time required to reach the steady state diverges. See Supplemental Material [44] for a full comparison between the time-domain dynamics from Eq. (2) and the response obtained from the truncated Green's-function formalism.

Finally, to qualitatively characterize device performance, we compute a signal-to-noise ratio  $\mathcal{S}_{\text{out}}(t)/\mathcal{N}_{\text{out}}(t)$ , defined by splitting the total number of output photons reflected from port  $\gamma$  when a unit-amplitude ( $\alpha_d = 1$ ) input coherent signal  $\langle d_{\text{in}}(t) \rangle = e^{-i\omega_d t}$  is injected at the same port, with all other ports remaining in vacuum,  $\langle d_{\text{out}}^\dagger(t) d_{\text{out}}(t) \rangle = \mathcal{S}_{\text{out}}(t) + \mathcal{N}_{\text{out}}(t)$ . Here, the first term corresponds to the coherent output signal, while the second accounts for output noise generated by the incoherent pump, and depend exclusively on  $R_{nm}(\bar{\omega})$  and  $P_{nm}(\bar{\omega})$  [44]. The resulting SNR exhibits a local maximum that saturates in the topological ideal case ( $\beta = 1$ ), corresponding to the boundary between stable (solid) and unstable (dashed) regions in Fig. 3.

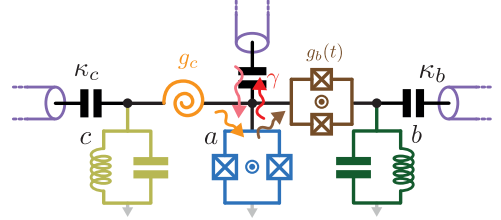


Figure 4. Schematic of a proposed cQED setup. The slow mode  $a$  couples to two fast-decaying auxiliary modes via flux-pumped Josephson elements. A dc SQUID mediates a time-modulated coupling  $g_b(t)$  to the lossy mode  $b$  (with decay  $\kappa_b$ ), while a SNAIL provides a parametric coupling  $g_c$  to the pumped mode  $c$  ( $\kappa_c$ ). Independent flux lines drive the SQUID at frequency  $\Omega$  and pump the SNAIL at a high-frequency  $\omega_p \simeq \omega_a + \omega_c$ .

*Implementation in cQED.*— The effective model discussed above could potentially be engineered in circuit QED by coupling a slow mode  $a$  to fast-decaying auxiliary resonators through flux-pumped Josephson nonlinear elements, see Fig. 4. For instance, a SNAIL [50, 51] provides a clean three-wave-mixing interaction when pumped at  $\omega_p \simeq \omega_a + \omega_c$ , while a flux-pumped dc SQUID operated in a four-wave-mixing regime implements an analogous interaction when  $2\omega_p \simeq \omega_a + \omega_c$  [52, 53]. When the auxiliary modes have large decay rates,  $\kappa_{\text{aux}} \gg g, \Omega, \kappa_a, P$ , they remain close to vacuum and can be adiabatically eliminated. This yields the effective time-dependent decay rate and incoherent pump used in our model,  $\kappa(t) = 4g_b^2(t)/\kappa_b$  and  $P = 4g_c^2/\kappa_c$ , where  $g_b(t)$  is a modulated beam-splitter coupling and  $g_c$  is a parametric pump coupling. These ingredients provide a straightforward and experimentally realistic route to realizing the Floquet topological frequency-conversion and amplification described in this work.

*Conclusions.*— We have shown that a single

driven-dissipative harmonic oscillator can host topological frequency conversion and amplification. Periodic modulation of its frequency and decay generates a non-Hermitian Floquet lattice with asymmetric hopping and a synthetic electric field. A local winding number in doubled space approximately predicts the full phase diagram, including the regime of directional gain and efficient frequency conversion. The associated singular vectors are well captured by Jackiw-Rebbi-type solitons emerging from Dirac cones in synthetic-frequency space. This mechanism is validated numerically and can be implemented, for instance, in circuit QED via modulated dissipation. Our work demonstrates that Floquet-engineered loss is an essential ingredient for enabling topological photonic functionality normally associated with higher-dimensional (physical or synthetic) systems. Looking ahead, this approach may prove useful in quantum-sensing applications and in extensions to richer architectures, ranging from parametrically driven single oscillators to higher-dimensional realizations via multichromatic drives and coupled-oscillator arrays.

A. P.-R. was initially supported by the Juan de la Cierva fellowship FJC2021-047227-I. Funding for A. P.-R. and P. G. is provided by the Swiss National Science Foundation through Project No. CRSII 222812/1. This research is part of the Munich Quantum Valley initiative, which is supported by the Bavarian state government with funds from the Hightech Agenda Bayern Plus. This work is supported by the Spanish projects PID2021-127968NBI00 and PID2024-159152NB-I00 (D.P. and M.C.R.), and by PID2023-146531NA-I00 (T.R. and A.G.L.), financed by MCIN/AEI/10.13039/501100011033 and ERDF/EU. T.R. further acknowledges the Ramón y Cajal program RYC2021-032473-I, financed by MCIN/AEI/10.13039/501100011033 and the European Union NextGenerationEU/PRTR.

---

\* [adrian.parra.rodriguez@gmail.com](mailto:adrian.parra.rodriguez@gmail.com)  
 † [diego.porras@csic.es](mailto:diego.porras@csic.es)

- [1] M. Z. Hasan and C. L. Kane, *Reviews of Modern Physics* **82**, 3045 (2010).
- [2] X.-L. Qi and S.-C. Zhang, *Reviews of Modern Physics* **83**, 1057 (2011).
- [3] L. Lu, J. D. Joannopoulos, and M. Soljačić, *Nature Photonics* **8**, 821 (2014).
- [4] T. Ozawa, H. M. Price, A. Amo, N. Goldman, M. Hafezi, L. Lu, M. C. Rechtsman, D. Schuster, J. Simon, O. Zilberman, and I. Carusotto, *Reviews of Modern Physics* **91**, 015006 (2019).
- [5] M. Jalali Mehrabad, S. Mittal, and M. Hafezi, *Physical Review A* **108**, 040101 (2023).
- [6] S. Barik, A. Karasahin, C. Flower, T. Cai, H. Miyake, W. DeGottardi, M. Hafezi, and E. Waks, *Science* **359**, 666 (2018).
- [7] C. J. Flower, M. J. Mehrabad, L. Xu, G. Moille, D. G. Suarez-Forero, O. Örsel, G. Bahl, Y. Chembo, K. Srinivasan, S. Mittal, and M. Hafezi, *Science* **384**, 1356 (2024).
- [8] A. Metelmann and A. A. Clerk, *Physical Review X* **5**, 021025 (2015).
- [9] K. Fang, J. Luo, A. Metelmann, M. H. Matheny, F. Marquardt, A. A. Clerk, and O. Painter, *Nature Physics* **13**, 465 (2017).
- [10] V. Peano, M. Houde, F. Marquardt, and A. A. Clerk, *Physical Review X* **6**, 041026 (2016).
- [11] A. McDonald, R. Hanai, and A. A. Clerk, *Physical Review B* **105**, 064302 (2022).
- [12] J. del Pino, J. J. Slim, and E. Verhagen, *Nature* **606**, 82 (2022).
- [13] J. H. Busnaina, Z. Shi, A. McDonald, D. Dubyna, I. Nsanzineza, J. S. C. Hung, C. W. S. Chang, A. A. Clerk, and C. M. Wilson, *Nature Communications* **15**, 3065 (2024).
- [14] J. J. Slim, C. C. Wanjura, M. Brunelli, J. Del Pino, A. Nunnenkamp, and E. Verhagen, *Nature* **627**, 767 (2024).
- [15] T. Ramos, A. Gómez-León, J. J. García-Ripoll, A. González-Tudela, and D. Porras, [arXiv:2207.13728v4 \[quant-ph\]](https://arxiv.org/abs/2207.13728v4) (2022).
- [16] K. Esaki, M. Sato, K. Hasebe, and M. Kohmoto, *Physical Review B* **84**, 205128 (2011).
- [17] Z. Gong, Y. Ashida, K. Kawabata, K. Takasan, S. Higashikawa, and M. Ueda, *Physical Review X* **8**, 031079 (2018).
- [18] D. Porras and S. Fernández-Lorenzo, *Physical Review Letters* **122**, 143901 (2019).
- [19] C. C. Wanjura, M. Brunelli, and A. Nunnenkamp, *Nature communications* **11**, 3149 (2020).
- [20] T. Ramos, J. J. García-Ripoll, and D. Porras, *Physical Review A* **103**, 033513 (2021).
- [21] C. C. Wanjura, M. Brunelli, and A. Nunnenkamp, *Physical Review Letters* **127**, 213601 (2021).
- [22] A. Gómez-León, T. Ramos, A. González-Tudela, and D. Porras, *Physical Review A* **106**, L011501 (2022).
- [23] Á. Gómez-León, T. Ramos, A. González-Tudela, and D. Porras, *Quantum* **7**, 1016 (2023).
- [24] M. Clavero-Rubio, T. Ramos, and D. Porras, *Physical Review Research* **7**, 043218 (2025).
- [25] N. H. Lindner, G. Refael, and V. Galitski, *Nature Physics* **7**, 490 (2011).
- [26] M. C. Rechtsman, J. M. Zeuner, Y. Plotnik, Y. Lumer, D. Podolsky, F. Dreisow, S. Nolte, M. Segev, and A. Szameit, *Nature* **496**, 196 (2013).
- [27] A. Gómez-León and G. Platero, *Physical Review Letters* **110**, 200403 (2013).
- [28] Y. Baum and G. Refael, *Physical Review Letters* **120**, 106402 (2018).
- [29] I. Martin, G. Refael, and B. Halperin, *Physical Review X* **7**, 041008 (2017).
- [30] J. Luneau, C. Dutreix, Q. Ficheux, P. Delplace, B. Douçot, B. Huard, and D. Carpentier, *Physical Review Research* **4**, 013169 (2022).
- [31] T. T. Koutsiperopoulos and R. Fleury, *Physical Review Letters* **120**, 087401 (2018).
- [32] M. Ritter, D. M. Long, Q. Yue, A. Chandran, and A. J. Kollár, [arXiv:2410.12908 \[quant-ph\]](https://arxiv.org/abs/2410.12908) (2024).
- [33] F. Ahrens, N. Crescini, A. Irace, G. Rastelli, P. Falferi,

A. Giachero, B. Margesin, R. Mezzena, A. Vinante, I. Carusotto, and F. Mantegazzini, *Physical Review A* **112**, 033506 (2025).

[34] N. Hatano and D. R. Nelson, *Physical Review Letters* **77**, 570 (1996).

[35] R. Jackiw and C. Rebbi, *Physical Review D* **13**, 3398 (1976).

[36] M. F. Atiyah and I. M. Singer, *Bulletin of the American Mathematical Society* **69**, 422 (1963).

[37] C. Callias, *Communications in Mathematical Physics* **62**, 213 (1978).

[38] S. Yao, Z. Yan, and Z. Wang, *Physical Review B* **96**, 195303 (2017).

[39] S. Yao and Z. Wang, *Physical Review Letters* **121**, 086803 (2018).

[40] P. J. D. Crowley, I. Martin, and A. Chandran, *Physical Review B* **99**, 064306 (2019).

[41] F. Koch and J. C. Budich, *Physical Review Research* **6**, 033124 (2024).

[42] F. Koch, Y.-M. Hu, and J. C. Budich, [arXiv:2511.16742 \[cond-mat.mes-hall\]](https://arxiv.org/abs/2511.16742) (2025).

[43] In a more general situation, e.g., if the auxiliary cavity were thermally occupied or driven, these  $\Omega/2$  sidebands would matter. Such cases can be conveniently treated by sampling the Floquet-Sambe space at spacing  $\Omega/2$ , avoiding the split definition of the noise operators in Eq. (5).

[44] See Supplemental Material.

[45] L. Herviou, J. H. Bardarson, and N. Regnault, *Physical Review A* **99**, 052118 (2019).

[46] A. Altland and M. R. Zirnbauer, *Physical Review B* **55**, 1142 (1997).

[47] R. Roy and F. Harper, *Physical Review B* **96**, 155118 (2017).

[48] R. Bianco and R. Resta, *Physical Review B* **84**, 241106 (2011).

[49] T. Kitagawa, E. Berg, M. Rudner, and E. Demler, *Physical Review B* **82**, 235114 (2010).

[50] N. E. Frattini, V. V. Sivak, A. Lingenfelter, S. Shankar, and M. H. Devoret, *Physical Review Applied* **10**, 054020 (2018).

[51] V. Sivak, N. Frattini, V. Joshi, A. Lingenfelter, S. Shankar, and M. Devoret, *Physical Review Applied* **11**, 054060 (2019).

[52] M. A. Castellanos-Beltran and K. W. Lehnert, *Applied Physics Letters* **91**, 083509 (2007).

[53] L. Planat, R. Dassonneville, J. P. Martínez, F. Foroughi, O. Buisson, W. Hasch-Guichard, C. Naud, R. Vijay, K. Murch, and N. Roch, *Physical Review Applied* **11**, 034014 (2019).

[54] A. J. Heeger, S. Kivelson, J. R. Schrieffer, and W. P. Su, *Reviews of Modern Physics* **60**, 781 (1988).

[55] P. Roushan, C. Neill, A. Megrant, Y. Chen, R. Babbush, R. Barends, B. Campbell, Z. Chen, B. Chiaro, A. Dunsworth, A. Fowler, E. Jeffrey, J. Kelly, E. Lucero, J. Mutus, P. J. J. O’Malley, M. Neeley, C. Quintana, D. Sank, A. Vainsencher, J. Wenner, T. White, E. Kapit, H. Neven, and J. Martinis, *Nature Physics* **13**, 146 (2017).

## END MATTER

*Topological description of periodically driven amplifiers.*— The Green's function in the Floquet–Sambe basis can be analyzed via the SVD of the dynamical matrix, which coincides with the eigensystem of the doubled Hermitian matrix defined in Eq. (7). A remarkable property of  $\mathcal{H}(\bar{\omega})$  is its chiral symmetry,  $\mathcal{S}\mathcal{H}(\bar{\omega})\mathcal{S} = -\mathcal{H}(\bar{\omega})$ , with  $\mathcal{S} = \mathbb{I} \otimes \sigma_z$ . In the most general case, the doubled Hamiltonian belongs to the AIII symmetry class, which can host topologically protected edge states.

To characterize these topological phases, we consider the translationally invariant (local) Hamiltonian Eq. (8), retaining the linear tilt, i.e.,  $f_{kk'} \approx n\delta_{kk'}$ . Working at the maximally nonreciprocal phase, i.e.,  $\phi = \pi/2$ , we can write the associated doubled-space dynamical matrix  $\tilde{\mathcal{H}}_k(\bar{\omega}, n) = r_x(k, n)\sigma_x + r_y(k, n)\sigma_y$  with

$$\begin{aligned} r_x(k, n) &= \bar{\omega} + \Omega(n + 2\eta_\omega \sin k), \\ r_y(k, n) &= \frac{\Omega(\eta_P - \eta_\gamma)}{2} - \frac{\Omega\eta_\kappa}{2}(1 + \cos k). \end{aligned} \quad (10)$$

The associated winding number (9), equivalent to

$$\nu_n(\bar{\omega}) = \oint \frac{dk}{2\pi} \frac{(\mathbf{r} \times \partial_k \mathbf{r})_z}{\|\mathbf{r}\|^2}, \quad (11)$$

is 0 or  $\pm 1$  depending on whether the trajectory of  $(r_x, r_y)$  encloses the origin. Furthermore, the sign of the winding number is sensitive to the curve orientation. In particular,  $\text{sgn}(\nu_n) = \text{sgn}(\sin(\phi))$ . Since this trajectory is an ellipse, non-trivial topology requires

$$\left(\frac{\bar{\omega} + n}{2\eta_\omega}\right)^2 + \left(\frac{\eta_P - \eta_\gamma - \eta_\kappa}{\eta_\kappa}\right)^2 \leq 1. \quad (12)$$

Using the defined normalized pump–loss imbalance ( $\beta \equiv (\eta_P - \eta_\gamma)/\eta_\kappa$ ), the topological condition becomes  $\left(\frac{\bar{\omega}}{\Omega} + n\right)^2 \leq (2\eta_\omega)^2 \beta(2 - \beta)$ . This inequality identifies when the local winding number is non-trivial,  $\nu_n \neq 0$ , namely for  $0 < \beta < 2$  and  $\eta_\omega, \eta_\kappa > 0$ . Physically,  $\beta$  quantifies the effective competition between incoherent pump and static losses, normalized by the strength of the modulated dissipation that induces asymmetric synthetic hopping. We stress that the modulation of both frequency and decay channels, via  $\eta_\omega$  and  $\eta_\kappa$ , is essential for obtaining non-trivial topology, i.e., without them, Eq. (12) traces a horizontal line rather than a closed loop.

Dynamical stability, on the other hand, requires net loss, i.e.,  $0 < \beta < 1$ . The intersection of these conditions determines a topological yet dynamically stable regime. Near the critical point  $\beta \simeq 1$ , where pump and loss nearly balance, the topological frequency-conversion window

$$\Delta n = 4\eta_\omega \sqrt{\beta(2 - \beta)}$$

reaches its maximal value  $\Delta n = 4\eta_\omega$ , corresponding to a conversion bandwidth  $\Delta\omega = 4\eta_\omega\Omega$ .

*Generalized Jackiw–Rebbi model.*— For simplicity and without loss of generality, we set  $\bar{\omega} = 0$  in the following analytical discussion. The doubled Hamiltonian corresponding to Eqs. (10) reads

$$\begin{aligned} \frac{\tilde{\mathcal{H}}_k(0, n)}{\Omega} &= (n + 2\eta_\omega \sin k)\sigma_x \\ &+ \frac{\eta_\kappa}{2}(\beta - 1 - \cos k)\sigma_y. \end{aligned} \quad (13)$$

Since  $\mathcal{H}(\bar{\omega})$  has a discrete chiral symmetry, the situation is analogous to the Su–Schrieffer–Heeger model for polyacetylene chains [54], where a topological soliton emerges at the interface between distinct dimerization patterns. Topological-insulator theory predicts that the soliton located at the ellipse boundary  $n_0 = \pm|2\eta_\omega \sqrt{\beta(2 - \beta)}|$ , corresponds to a zero-singular-value eigenstate of  $\mathcal{H}(\bar{\omega})$ , separated from the continuum by a finite gap. This behavior directly mirrors the JR mechanism for a Dirac particle with a spatially varying mass.

Exploiting the chiral (sublattice) symmetry, the spectrum consists of pairs of eigenvalues  $E(k, n) = \pm s_k(n)$ , where  $s_k(n) \geq 0$  denotes the singular value of  $\tilde{\mathcal{H}}_k(n)$ . The inequivalent minima of  $s_k(n)$  occur at the two points  $(+k_0, -n_0)$  and  $(-k_0, +n_0)$ , where

$$\begin{aligned} k_0 &= |\arccos(\beta - 1)|, \\ n_0 &= |2\eta_\omega \sin k_0| = |2\eta_\omega \sqrt{1 - (\beta - 1)^2}|. \end{aligned} \quad (14)$$

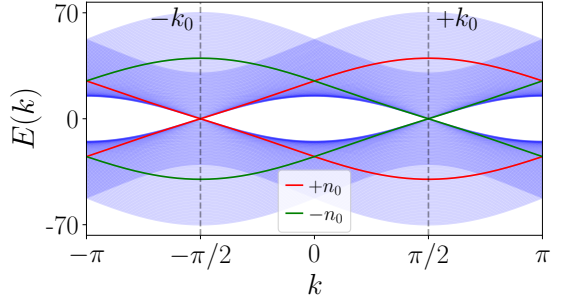


Figure 5. Eigenvalues of the doubled matrix  $\tilde{\mathcal{H}}_k(0, n)$  for different values of  $n \in [-50, 50]$  and  $\beta = 1$ . The plot shows the presence of two Dirac cones at the values  $(+k_0, -n_0)$  and  $(+k_0, +n_0)$ . The above figure is computed for the following parameters  $\eta_P = 20s$ ,  $\eta_\omega = \eta_\gamma/s = \eta_\kappa/s = 10$ ,  $\phi = \pi/2$ ,  $\bar{\omega} = 0$ , and  $s = 3$ .

*Left solitonic solution.*— We expand around the minimum  $(+k_0, -n_0)$  to obtain the left solitonic solution on the  $n$ -axis by writing  $k = k_0 + \delta k$ ,  $|\delta k| \ll 1$ . The Hamiltonian linearized around this point reads

$$\frac{\tilde{\mathcal{H}}_{\delta k}(0, n)}{\Omega} \approx (n + n_0 + A(\beta)\delta k)\sigma_x + B(\beta)\delta k\sigma_y, \quad (15)$$

with the coefficients

$$A(\beta) \equiv 2\eta_\omega \cos k_0 = 2\eta_\omega(\beta - 1), \quad (16)$$

$$B(\beta) \equiv \frac{\eta_\kappa}{2} \sin k_0 = \frac{\eta_\kappa}{2} \sqrt{\beta(2 - \beta)}. \quad (17)$$

This procedure implements a slowly-varying-envelope (continuum) approximation of the discrete Floquet-Sambe matrix  $\hat{H}_{nm}$  from Eq. (4). States in the synthetic-frequency basis,  $\psi_n$ , are represented via a Fourier transform centered around  $k_0$ :

$$\psi_n = \frac{1}{\sqrt{2\pi}} \int_{\mathbb{R}} d(\delta k) e^{i(k_0 + \delta k)n} \psi(\delta k). \quad (18)$$

Here  $\psi(\delta k)$  varies smoothly over the relevant momentum range. To make explicit the slowly-varying-envelope approximation, we factor out from the above expression the fast Bloch oscillations and define a smooth envelope  $\varphi(n)$  via

$$\psi_n = e^{ik_0 n} \varphi(n), \quad (19)$$

where  $\varphi(n) = \frac{1}{\sqrt{2\pi}} \int_{\mathbb{R}} d(\delta k) e^{i\delta k n} \psi(\delta k)$  changes only over many synthetic-frequency sites. For notational simplicity, we will simply write  $\varphi(n) \equiv \psi(n)$ . Under this assumption, neighboring components satisfy

$$\psi_{n \pm 1} \simeq e^{\pm i k_0} [\psi(n) \pm \partial_n \psi(n)]. \quad (20)$$

In momentum space, this is equivalent to a linear expansion of  $\sin(k_0 + \delta k)$  and  $\cos(k_0 + \delta k)$ , retaining only first-order terms in  $\delta k$ . Formally, the mapping  $\delta k \mapsto -i\partial_n$  converts the discrete Hamiltonian into a continuous effective Hamiltonian, valid for slowly-varying components. This approximation relies on three assumptions: (i)  $|\delta k| \ll 1$ , (ii) the envelope varies slowly over several lattice sites, and (iii) higher-order corrections in  $\delta k$  or  $\delta n_R$  are negligible.

Applying this correspondence, the effective continuous Hamiltonian reads

$$\frac{\tilde{\mathcal{H}}_{\text{eff}}(0, n)}{\Omega} \approx (n + n_0 - iA\partial_n)\sigma_x - iB\partial_n\sigma_y, \quad (21)$$

which represents a modified JR Hamiltonian, with two independent velocities  $A(\beta)$  and  $B(\beta)$ , that make the zero mode complex in general. We seek localized (*solitonic*) zero-energy solutions to  $\tilde{\mathcal{H}}_{\text{eff}}(0, n)\psi = 0$  with  $\psi = (u, v)^T$ . The two components satisfy

$$\begin{aligned} (n + n_0)v - (iA + B)\partial_n v &= 0, \\ (n + n_0)u - (iA - B)\partial_n u &= 0, \end{aligned} \quad (22)$$

with Gaussian solutions

$$v(n) = \mathcal{N}_v e^{\frac{(n+n_0)^2}{2(iA+B)}}, \quad u(n) = \mathcal{N}_u e^{\frac{(n+n_0)^2}{2(iA-B)}}. \quad (23)$$

Only  $u(n)$  is normalizable, since  $B > 0$ . Hence,

$$\psi_L = \begin{pmatrix} u(n) \\ 0 \end{pmatrix}, \quad u(n) = \mathcal{N}_u e^{-\frac{(n+n_0)^2}{2\sigma_r^2}} e^{-i\frac{(n+n_0)^2}{2\sigma_i^2}}. \quad (24)$$

The Gaussian widths are given in terms of the velocities by

$$\sigma_r^2 = \frac{A^2 + B^2}{|B|}, \quad \sigma_i^2 = \frac{A^2 + B^2}{A}, \quad (25)$$

and the normalization constant is  $\mathcal{N}_u = (\pi\sigma_r^2)^{-1/4}$ .

*Right solitonic solution.* A similar procedure can be developed by expanding around the minimum  $(-k_0, +n_0)$  for the solitonic solution on the right. Let  $k = -k_0 + \delta k$  so that we get a pair of analogous equations to (22), with  $(n + n_0) \rightarrow (n - n_0)$  after promoting to the continuum, where only  $v(n)$  is normalizable since now  $B < 0$ . Hence,

$$\psi_R = \begin{pmatrix} 0 \\ v(n) \end{pmatrix}, \quad v(n) = \mathcal{N}_v e^{-\frac{(n-n_0)^2}{2\sigma_r^2}} e^{-i\frac{(n-n_0)^2}{2\sigma_i^2}}, \quad (26)$$

with the same normalization constant as in the previous case  $\mathcal{N}_v = \mathcal{N}_u$ .

The real and imaginary parts of the Gaussian width determine, respectively, the localization and phase curvature of the soliton. Explicitly, using  $r = \eta_\kappa/\eta_\omega$ ,

$$\frac{1}{\sigma_r^2} = \frac{r}{2\eta_\omega} \frac{\sqrt{\beta(2-\beta)}}{4(\beta-1)^2 + \frac{r^2}{4}[\beta(2-\beta)]}, \quad (27)$$

$$\frac{1}{\sigma_i^2} = \frac{1}{\eta_\omega} \frac{2(\beta-1)}{4(\beta-1)^2 + \frac{r^2}{4}[\beta(2-\beta)]}. \quad (28)$$

At the symmetric point  $\beta = 1$ , the imaginary width contribution vanishes and one recovers the original Jackiw-Rebbi solitons, characterized by

$$\sigma_r|_{\beta=1} = \sqrt{\eta_\kappa/2}, \quad 1/\sigma_i^2|_{\beta=1} = 0. \quad (29)$$

We can mention in passing that these continuous Gaussian solitonic solutions are self-consistently justified when  $\sigma_{r,i} \gg 1$ . Interestingly, we observe that the shape of the Gaussian-like singular vectors is increasingly well captured for fixed  $\beta$  as  $r \rightarrow \infty$ .

Summarizing, topology emerges from the sign change of the effective mass term ( $m(n) = n \mp n_0$ ) in the continuum Dirac description generated by the doubled Hamiltonian  $\tilde{\mathcal{H}}_{\text{eff}}$ . This mass inversion produces localized states in the synthetic-frequency dimension, in direct analogy with Jackiw-Rebbi solitons bound to domain walls [35]. The two symmetry-related minima ( $\pm k_0, \mp n_0$ ) produce two independent Dirac Hamiltonians with opposite chirality, each hosting a single normalizable zero mode predicted by the index theorem [37]. This provides a unified and compact topological explanation for the appearance of protected solitonic states in the synthetic-frequency dimension of the driven amplifier.

## Supplemental Material for “Floquet Topological Frequency-Converting Amplifier”

Adrian Parra-Rodriguez<sup>1,2,3,4</sup>, Miguel Clavero-Rubio<sup>1</sup>, Philippe Gigon<sup>2,3,4</sup>, Tomás Ramos<sup>1</sup>, Álvaro Gómez-León<sup>1</sup>, Diego Porras<sup>1</sup>

<sup>1</sup>*Instituto de Física Fundamental (IFF), CSIC, Calle Serrano 113b, 28006 Madrid, Spain* <sup>2</sup>*Technical University of Munich, TUM School of Natural Sciences, Physics Department, 85748 Garching, Germany*

<sup>3</sup>*Walther-Meissner-Institut, Bayerische Akademie der Wissenschaften, 85748 Garching, Germany*

<sup>4</sup>*Munich Center for Quantum Science and Technology (MCQST), 80799 Munich, Germany*

### ADIABATIC ELIMINATION

Here we derive the time-dependent quantum Langevin equation presented in Eq. (2) of the main text, starting from a microscopic model in which the system mode  $a$  is coupled to rapidly decaying auxiliary bosonic modes. A time-dependent coupling to one auxiliary mode generates an effective modulated decay channel for  $a$ , while a parametric coupling to a second fast-decaying mode yields an incoherent pump. Both constructions rely on standard adiabatic elimination in the Born-Markov regime.

#### Time-dependent decay channel

We first consider a single auxiliary mode  $b$  that mediates time-dependent decay. The full system is governed by the Hamiltonian

$$H = \omega_a a^\dagger a + \omega_b b^\dagger b + g_b(t)(a^\dagger b + ab^\dagger), \quad (\text{S1})$$

where  $g_b(t) = g_{b0} \cos(\Omega t/2)$  is a real-valued time-periodic coupling. The mode  $b$  is coupled to a Markovian bath, resulting in fast decay at rate  $\kappa_b$ , and is taken to be initially in its vacuum state. We also allow mode  $a$  to have its own intrinsic loss and (possibly) gain channels, as detailed in the main text.

We move to an interaction picture with respect to the free evolution of the uncoupled modes, defined by

$$U_0(t) = \exp[-i(\omega_a a^\dagger a + \omega_b b^\dagger b)t]. \quad (\text{S2})$$

In this frame, the interaction Hamiltonian becomes

$$\tilde{H}_I(t) = -ig_b(t)(a^\dagger b e^{i\Delta_b t} - ab^\dagger e^{-i\Delta_b t}), \quad (\text{S3})$$

with  $\Delta_b = \omega_b - \omega_a$  the detuning between the two modes. The Heisenberg equations of motion in this interaction picture are

$$\dot{a}(t) = -g_b(t)e^{i\Delta_b t}b(t), \quad (\text{S4})$$

$$\dot{b}(t) = g_b(t)e^{-i\Delta_b t}a(t) - \frac{\kappa_b}{2}b(t) + \sqrt{\kappa_b}b_{\text{in}}(t), \quad (\text{S5})$$

where  $b_{\text{in}}(t)$  is the input noise operator driving the lossy auxiliary mode, with  $[b_{\text{in}}(t), b_{\text{in}}^\dagger(t')] = \delta(t - t')$ .

We assume that the decay rate  $\kappa_b$  is large compared to all other relevant energy scales

$$\kappa_b \gg g_{b0}, \Omega, \kappa_a, P, \quad (\text{S6})$$

so that  $b$  can be adiabatically eliminated. Formally integrating the equation for  $b(t)$  yields

$$b(t) \approx \int_0^\infty d\tau e^{-\frac{\kappa_b}{2}\tau} \left[ g_b(t - \tau)e^{-i\Delta_b(t - \tau)}a(t - \tau) + \sqrt{\kappa_b}b_{\text{in}}(t - \tau) \right]. \quad (\text{S7})$$

Inserting this expression into the equation for  $\dot{a}(t)$ , and assuming that  $g_b(t)$  and  $a(t)$  vary slowly on the timescale  $\kappa_b^{-1}$ , we use the Markov approximation  $g_b(t - \tau) \approx g_b(t)$  and  $a(t - \tau) \approx a(t)$  inside the integral. Evaluating the convolution yields

$$\dot{a}(t) = -\underbrace{\frac{g_b(t)^2}{\kappa_b/2 - i\Delta_b}}_{\Gamma_b(t)} a(t) - g_b(t)e^{i\Delta_b t}\sqrt{\kappa_b} \int_0^\infty d\tau e^{-\frac{\kappa_b}{2}\tau} b_{\text{in}}(t - \tau). \quad (\text{S8})$$

Writing  $\Gamma_b(t) = \kappa(t)/2 + i\delta\omega(t)$ , we identify the induced time-dependent decay rate and Lamb shift as

$$\kappa(t) = \frac{4g_b(t)^2}{\kappa_b^2 + 4\Delta_b^2} \kappa_b, \quad \delta\omega(t) = \frac{4g_b(t)^2}{\kappa_b^2 + 4\Delta_b^2} \Delta_b. \quad (\text{S9})$$

On resonance ( $\Delta_b = 0$ ), this simplifies to

$$\kappa(t) = \frac{4g_b(t)^2}{\kappa_b}. \quad (\text{S10})$$

The second term in Eq. (S8) represents an effective input-noise contribution, which can be written as a filtered noise operator. On resonance, it is well-approximated by

$$\xi_{\text{aux}}(t) = -g_b(t)\sqrt{\kappa_b} \int_0^\infty d\tau e^{-\frac{\kappa_b}{2}\tau} b_{\text{in}}(t-\tau) \approx -\frac{2g_b(t)}{\sqrt{\kappa_b}} b_{\text{in}}(t), \quad (\text{S11})$$

consistent with an effective decay channel of rate  $\kappa(t)$ .

### Incoherent pump channel

An incoherent pump channel for  $a$  can be engineered in a fully analogous way by coupling  $a$  to a second fast-decaying auxiliary mode  $c$  via a parametric (two-mode-squeezing) interaction [S13, S55],

$$H_P = \omega_c c^\dagger c + g_c(a^\dagger c^\dagger + ac), \quad (\text{S12})$$

with  $c$  coupled to a Markovian bath at rate  $\kappa_c$  and initialized in its vacuum state. Working in the appropriate rotating frame and applying the same adiabatic-elimination steps as above (now for  $c$ ), one finds that for

$$\kappa_c \gg g_c, \kappa_a, \kappa_b, \Omega, \quad (\text{S13})$$

the mode  $c$  induces an effective incoherent pump for  $a$  with rate

$$P = \frac{4g_c^2}{\kappa_c}, \quad (\text{S14})$$

and an associated noise term  $\sqrt{P} c_{\text{in}}^\dagger(t)$ , where  $c_{\text{in}}(t)$  denotes the corresponding input noise operator. This is the standard result for a negative-damping (gain) channel generated via a strongly damped parametric auxiliary mode.

### Full effective Langevin equation

Including the intrinsic loss of mode  $a$ , the engineered time-dependent decay from mode  $b$ , and the incoherent pump from mode  $c$ , and restoring the possibly time-dependent system frequency  $\omega_0(t)$ , we obtain the effective Langevin equation

$$\dot{a}(t) = -i\omega_0(t)a(t) + \frac{P - (\gamma + \kappa(t))}{2} a(t) + \xi_{\text{in}}(t), \quad (\text{S15})$$

with  $\kappa(t) = \frac{4g_b(t)^2}{\kappa_b}$ , where  $\gamma$  denotes any additional unmodulated loss channel. The total input noise operator is

$$\xi_{\text{in}}(t) = -\sqrt{\kappa(t)} b_{\text{in}}(t) - \sqrt{\gamma} d_{\text{in}}(t) + \sqrt{P} c_{\text{in}}^\dagger(t), \quad (\text{S16})$$

with  $d_{\text{in}}$  the input associated with the background loss channel. This Langevin equation coincides with Eq. (2) in the main text and provides a microscopic justification for the effective model with time-dependent decay rate  $\kappa(t)$  and incoherent pump  $P$ . The derivation is valid in the regime  $\kappa_{b,c} \gg g_{b0}, g_c, \Omega, \kappa_a$  and under the usual Markov and adiabatic approximations, and it extends straightforwardly to more general slow modulations of  $g_b(t)$  and  $\omega_0(t)$ .

As an example, in Fig. S1(a) we show a comparison between the transient of the real part of the averaged field amplitude  $\alpha(t) = \langle a(t) \rangle$  computed by direct integration of the Langevin equation with a coherent input at port  $\gamma$ ,

$\langle d_{\text{in}}(t) \rangle = \alpha_d e^{-i\omega_d t}$  ( $\omega_d = \bar{\omega}_d + n_d \Omega$ ) with  $\alpha_d = \frac{\epsilon_d}{\sqrt{\gamma}}$ , and all others in vacuum, with the reconstructed signal obtained from the Green's function formalism (Eq. (3)), i.e.,

$$\langle \bar{a}_n(\bar{\omega}) \rangle = \sqrt{2\pi} \epsilon_d \mathbf{G}_{n,n_d}(\bar{\omega}) \delta(\bar{\omega} - \bar{\omega}_d). \quad (\text{S17})$$

In Fig. S1(b), we show the time-integrated dynamics for the one-mode model and a more realistic three-mode model in cQED, with the two auxiliary modes in the very bad-cavity limit. Naturally, as we approach the topological singular regime ( $\beta = 1$ ) the auxiliary degrees of freedom become populated and the effective slow-dynamics deviates from the idealized case.

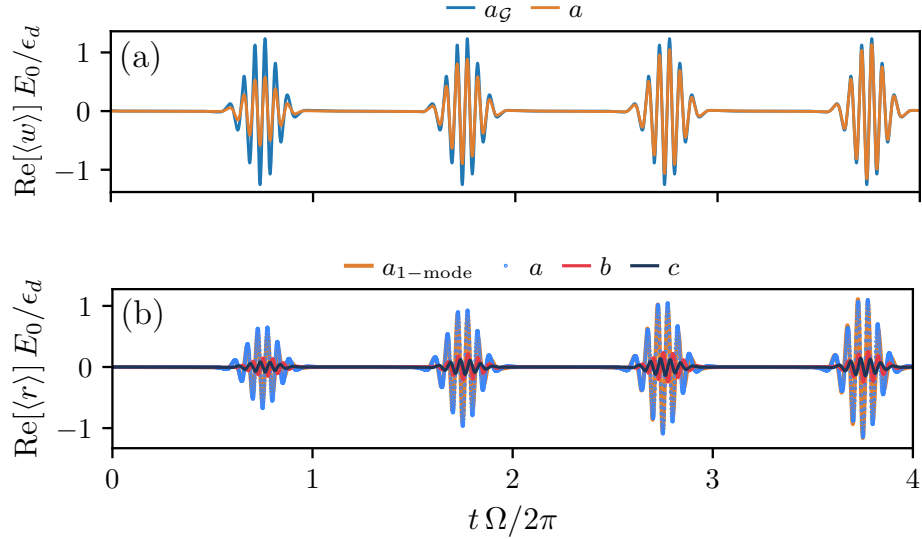


Figure S1. (a) Transient dynamics for the real part of the averaged fields  $\langle w(t) \rangle$ , with  $w \in \{a, a_G\}$ . The curve for the integrated Langevin equation (2),  $w = a$  (orange) approaches the steady-state response  $w = a_G$  (blue), obtained from the truncated Green's function in Eq. (S17). Both quantities are normalized by the drive amplitude  $\epsilon_d$  and by the singular value  $|E_0| \approx 2.4 \times 10^{-3}$ . Parameters are  $\eta_\omega = \eta_\kappa = \eta_\gamma = 10$ ,  $\eta_P = 19.8$  ( $\beta = 0.98$ ), and  $\phi = \pi/2$ . As  $\beta \rightarrow 1$ , the system requires increasingly long times to reach its steady state. (b) Time-domain comparison between the real part of the amplitudes in the three-mode model ( $r = \{a, b, c\}$ ), and those of the effective (ideal) one-mode model ( $r = \{a_{1\text{-mode}}\}$ ). The parameters used for  $a_{1\text{-mode}}$  (and  $a$ ) are the same as in panel (a). The  $b$  and  $c$  modes are resonant with  $a$  and decay at rates  $\kappa_b = 200\Omega$  and  $\kappa_c = 1200\Omega$ , with couplings  $g_b(t)$  and  $g_c$  chosen to reproduce  $\eta_\kappa$  and  $\eta_P$ .

## SIGNAL-TO-NOISE RATIO

In this section, we first compute the signal-to-noise ratio if we measure the photon number. Using the input-output relation at the static port  $\gamma$ , the Floquet-Sambe components of the output field read

$$\bar{d}_{\text{out},n}(\bar{\omega}) = \sum_m \left[ \mathbf{R}_{nm}(\bar{\omega}) \bar{d}_{\text{in},m}(\bar{\omega}) + \mathbf{P}_{nm}(\bar{\omega}) \bar{h}_{\text{in},-m}^\dagger(-\bar{\omega}) + \mathbf{Q}_{nm}(\bar{\omega}) \bar{a}_{\text{in},m}(\bar{\omega}) \right], \quad (\text{S18})$$

with coefficient matrices

$$\mathbf{R}_{nm}(\bar{\omega}) = \delta_{nm} - i\Omega \eta_\gamma \mathbf{G}_{nm}(\bar{\omega}), \quad \mathbf{P}_{nm}(\bar{\omega}) = i\Omega \sqrt{\eta_P \eta_\gamma} \mathbf{G}_{nm}(\bar{\omega}). \quad (\text{S19})$$

For simplicity, we assume that the  $\kappa(t)$  port is in vacuum and omit the definition of  $\mathbf{Q}_{nm}(\bar{\omega})$ ; it follows straightforwardly from a Floquet-Fourier expansion with  $\Omega/2$  spacing.

We now consider the case where the port  $\gamma$  is driven with a monochromatic coherent tone  $|\alpha(\omega_d)\rangle$  at  $\omega_d = \bar{\omega}_d + n_d \Omega$ , such that  $\langle \bar{d}_{\text{in},m}(\bar{\omega}) \rangle = \sqrt{2\pi} \alpha_d \delta_{m,n_d} \delta(\bar{\omega} - \bar{\omega}_d)$ , while all other inputs remain in vacuum. The output photon flux can be split into a coherent contribution (*signal*) and an incoherent one (*noise*),

$$\mathcal{D}_{\text{out}}(t) \equiv \langle d_{\text{out}}^\dagger(t) d_{\text{out}}(t) \rangle = \mathcal{S}_{\text{out}}(t) + \mathcal{N}_{\text{out}}(t), \quad (\text{S20})$$

with (cyclostationary) components

$$\mathcal{S}_{\text{out}}(t) = \left| \alpha_d \sum_n e^{-in\Omega t} \mathsf{R}_{n,n_d}(\bar{\omega}_d) \right|^2, \quad (\text{S21})$$

$$\mathcal{N}_{\text{out}}(t) = \frac{1}{2\pi} \sum_{n,m} e^{i(n-m)\Omega t} \sum_l \int_0^\Omega d\bar{\omega} \mathsf{P}_{nl}^*(\bar{\omega}) \mathsf{P}_{ml}(\bar{\omega}), \quad (\text{S22})$$

where only the incoherent-pump bath contributes to  $\langle a^\dagger a \rangle$ , since the other input ports are at zero-temperature and enter exclusively through the matrix  $\mathsf{P}_{nm}$ .